Available online at www.sciencedirect.com
SCIENCE DIRECT
Catalysis Today 116 (2006) 271–280
CATALYSIS TODAY
www.elsevier.com/locate/cattod

Characterization of NiAl and NiCuAl catalysts prepared by different methods for hydrogen production by thermo catalytic decomposition of methane

I. Suelves, M.J. Lázaro [a], R. Moliner [a], Y. Echegoyen [a], J.M. Palacios [b,*]

[a] *Instituto de Carboquímica CSIC, Miguel Luesma Castán 4, 50015 Zaragoza, Spain*
[b] *Instituto de Catálisis y Petroleoquimica CSIC, Campus Universidad Autonoma. Cantoblanco, 28049 Madrid, Spain*

Abstract

NiAl and NiCuAl catalysts have been prepared by co-precipitation, fusion and impregnation methods to promote the Ni formation, as active phase, in different degrees of dispersion and crystal domain sizes as evidenced through the characterization study of fresh catalysts. Performance tests show that the hydrogen production was not highly dependent on the preparation method used but the presence of Cu as a dopant in NiCuAl catalysts enhanced the catalytic activity substantially. The catalyst deactivation was never reached at the fixed times used in the reactivity tests. The Ni properties, mostly derived from thermal sintering and chemical-induced faceting were substantially altered during the process of methane decomposition, and the properties of the deposited carbon were highly dependent on the presence of Cu as a dopant in NiCuAl catalysts. NiCuAl catalysts enhances the formation of a well-ordered graphitic carbon while NiAl catalysts promote the deposition of a turbostratic carbon suitable as catalytic supports or hydrogen storage.

Keywords: Methane; Hydrogen production; Ni catalysts; Carbon; Structural properties

1. Introduction

Hydrogen is an ideal good energy vector and the suitable feeding gas for fuel cells operating at low temperatures [1,2]. An alternative process for hydrogen production to conventional steam reforming is the thermal decomposition of methane as main component of natural gas:

$$CH_4 \rightarrow C + H_2$$

This endothermic reaction has no side-reactions and according to thermodynamic data [3] high methane conversions can be achieved at operating temperatures above 900 °C. Although with lower methane conversions, the reaction rate still could be high enough at lower temperatures using suitable catalysts, such as transition metals.

At high reaction rates several studies have shown that the deposited carbon leads to rapid catalyst deactivation [3] through the formation of uniform coatings on the catalyst surface. At lower reaction rates, however, carbon is deposited as long filaments and catalyst deactivation may be delayed to times when the carbon concentration on catalyst is very high [4–6].

Most studies concerned with the thermal decomposition of methane have used Ni catalysts [7–12]. The process starts with the methane adsorption on Ni surface and subsequent rupture of C–H bonds. Theoretical DFT calculations show that the methane chemisorption is favoured on high-index Ni faces, like (1 1 0), (2 1 0), with relatively high surface energy [13]. On the contrary, carbon growth is enhanced on low-index faces (1 1 1) and (1 0 0) exhibiting a lower mismatch with the graphite lattice. Consequently, all mechanisms proposed in the literature for the growth of filamentous carbon on the surface of transition metals assume the presence of catalyst particles exhibiting a high anisotropy of shape: Ni particles exposing high-index faces showing a rounded appearance on which the catalytic decomposition of methane takes place together with low-index faces exhibiting polyhedral appearance on which the deposited carbon emerges as long filaments. Since carbon deposition and filaments growth take place in different crystal faces of the Ni particle, the deposited carbon has to diffuse from one region to other of the particle during the decomposition process [14–16].

* Corresponding author. Tel.: +34 915854787; fax: +34 915854760.
E-mail address: jmpalacios@icp.csic.es (J.M. Palacios).

0920-5861/$ – see front matter © 2006 Elsevier B.V. All rights reserved.
doi:10.1016/j.cattod.2006.05.071

Independently if carbon transport takes place through bulk diffusion, in fact carbide species only have been detected using Fe catalysts [17], or, more probably, through surface diffusion, this mechanism only can be operative at relatively highly constrained operating conditions. The rate of carbon deposition must be low enough to prevent accumulation at the leading face allowing carbon migration and subsequent filament growth in the opposite side. If the deposition rate is excessively high, carbon grows as uniform coatings that rapidly lead to catalyst deactivation [3].

This mechanism predicts that the size and shape of catalyst particles must have a high influence in the thermal decomposition of methane. In spite of that, relatively few efforts have been addressed to study these effects and references in the literature are relatively scarce. Some studies have shown that small Ni particles are rapidly deactivated while the largest ones exhibit low activities being 34 nm the optimum size [18].

In this paper, NiAl and NiCuAl catalysts with different Ni contents have been prepared using different methods including co-precipitation, fusion and impregnation, for the thermal decomposition of methane. Presumably, these different preparation methods will promote the formation of Ni with different particle sizes exposing different crystal faces that probably will affect the catalytic process. The activity tests have been carried out in a fixed-bed reactor and the catalyst performance assessed by measurements of the hydrogen evolution along the tests and of the total carbon deposited at the end of the test. The properties of the fresh and used catalysts as well as the nature of the deposited carbon have been studied with the aim of catalyst optimisation in hydrogen production by achieving Ni catalysts with life time as long as possible. The structural properties of the deposited carbon are also studied in order to find potential industrial applications for this product.

2. Experimental

2.1. Catalyst preparation

Ni and NiCu on alumina fresh catalysts have been prepared by different methods including co-precipitation, fusion and impregnation widely described in the literature [6,10,11]. Co-precipation catalysts were prepared by co-precipitation of their respective soluble nitrates in an aqueous solution and the precipitates subsequently washed, dried and calcined at 450 °C. Impregnation catalysts were prepared by impregnation with an aqueous solution of aluminium nitrate, of a powder mixture of nickel and copper oxides previously obtained by thermal decomposition of their respective nitrates. Fusion catalysts were prepared by direct powder mixture of their respective nickel, copper and aluminium nitrates followed by calcination at 350 °C.

2.2. Characterization techniques

Morphological appearance, chemical composition, Ni distribution and chemical association of Ni and Cu in fresh and used catalysts after activity tests have been studied in an scanning electron microscope (SEM) ISI DS-130 coupled to a PGT Prism Si/Li detector disposed with ultrathin window for chemical analysis by energy dispersive X-ray (EDX). The identification of crystalline phases and measurement of crystal domain sizes of Ni and deposited carbon through subsequent processing of diffraction patterns by Rietveld methods, have been carried out in a diffractometer Seifert 3000 using Ni-filtered Cu Kα radiation for obtaining the respective powder X-ray diffraction (XRD) patterns. Raman spectra for the structural characterization of deposited carbon in used catalysts have been acquired in a Raman spectrometer using a laser beam as excitation of 20 mW and $\lambda = 514$ nm coupled to an optical system allowing spectra acquisition from areas about 1 μm^2. High resolution electron microscopy (HREM) of the fresh and used catalysts were obtained in a transmission electron microscope (TEM) JEOL JEM-3010 operating at accelerating voltage of 300 kV, using a hot field emission cathode as electron source and an objective lens with spherical and chromatic aberration constants $C_s = 0.5$ mm and $C_c = 1.1$ mm, respectively, to achieve a point resolution of 0.2 nm.

2.3. Activity tests

Activity tests were run in a fixed-bed quartz reactor 2 cm i.d., 60 cm height, filled with 0.3 g of catalyst, using a flow rate of pure CH_4 of 20 cm^3/min as feeding gas at reaction temperature of 700 °C. Prior to activity tests, all catalysts were subjected to a reduction pre-treatment with a flow rate of pure hydrogen of 20 cm^3/min for 3 h at two reduction temperatures of 550 or 650 °C. The composition of the outlet gas from the reactor was determined by gas chromatography using two packed columns, Molecular Sieve 13× and Porapack, and a thermal conductivity detector (TCD). Using this detection system, no methane decomposition products other than hydrogen, as a major reaction product, was detected in the outlet gas. The evolution of CO and CO_2 has also been studied by connecting the two packed columns to a catalytic hydrogenation reactor and equipping the gas chromatograph with an additional flame ionization detector (FID). In this case, levels of carbon oxides gases in the range of ppmv were also measured. Deposited carbon-to-Ni weight ratios at the end of the tests were approximately estimated from sample weight differences.

3. Results and discussion

3.1. Characterization of the calcined and pre-reduced fresh catalysts

The composition of the fresh catalysts determined by SEM–EDX is shown in Table 1. Ni and presumably Cu are the active phases for the thermal decomposition of methane. Al_2O_3 is inactive only present to increase the degree of dispersion of the Ni-containing phases [9,19–22]. Additionally, most of the mechanical properties exhibited by the prepared catalysts are due to the presence of this inactive phase. The Ni concentration in the prepared samples is highly variable while the Cu-to-Ni

Table 1
Chemical composition and domain size of NiO in the fresh calcined samples

Muestras	SEM–EDX		XRD (NiO domain size (nm))
	$(Ni/Al)_{at}$	$(Cu/Ni)_{at}$	
CopNiAl	1.0		4
FusNiAl	3.7		24
ImpNiAl	4.5		25
CopNiCuAl	3.6	0.16	6
FUSNiCuAl	6.6	0.12	22
ImpNiCuAl	4.7	0.11	31

atomic ratio in NiCuAl catalysts was almost constant (11–16 at.%). The powder XRD patterns of the fresh calcined catalysts reveal the presence of NiO as the only nickel containing phase detected. Alumina was only detected through the presence of some characteristic broad reflections in some samples since it is microcrystalline. The crystal domain size of NiO in calcined fresh catalysts determined through further processing of powder XRD patterns by Rietveld methods is also shown in Table 1. As expected it is highly dependent on the method of catalyst preparation used: At one side, coprecipitation seems to enhance the formation of NiO with small domain sizes while fusion and impregnation, on the other side, promote the formation of relatively large NiO crystals. Additionally, the presence of Cu increases slightly the domain size of NiO in NiCu catalysts. Since no Cu containing phase was detected by XRD, Cu is supposed to be present as a mixed oxide $Ni_{(1-x)}Cu_xO$, with identical structure than NiO in which Cu partially substitutes to Ni.

The powder XRD patterns of the fresh catalysts after applying a reduction pre-treatment under a H_2 flow at 550 or 650 °C are shown in Fig. 1. The two prominent reflections shown in the patterns in this angle range are assigned to metallic Ni planes (1 1 1) and (2 0 0). Obviously, metallic Ni comes from hydrogen reduction of NiO that was present in the calcined fresh catalysts. However, a weak reflection at 43.32° assigned to NiO is evidenced, especially in the reduced sample at 550 °C ImpNiAl550 (Fig. 1). Its presence is probably due to partial Ni oxidation by air exposition of samples in the time interval on passing from reactor to diffractometer. It is worth

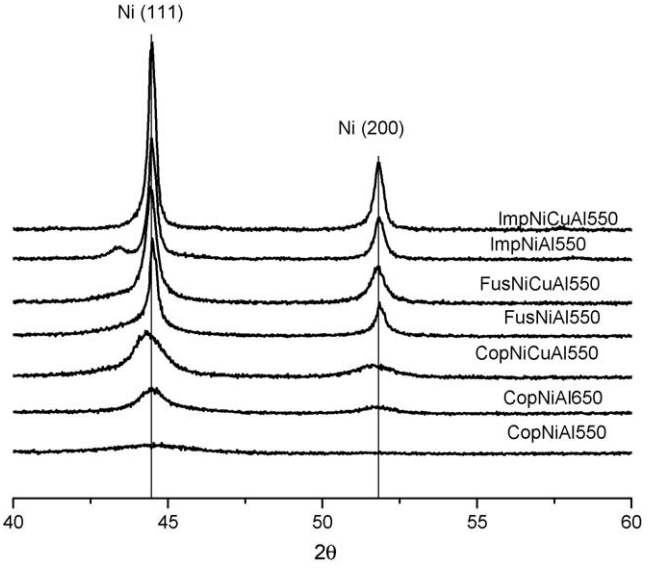

Fig. 1. Powder XRD patterns of fresh catalysts after reduction pre-treatment in hydrogen flow at 550 or 650 °C.

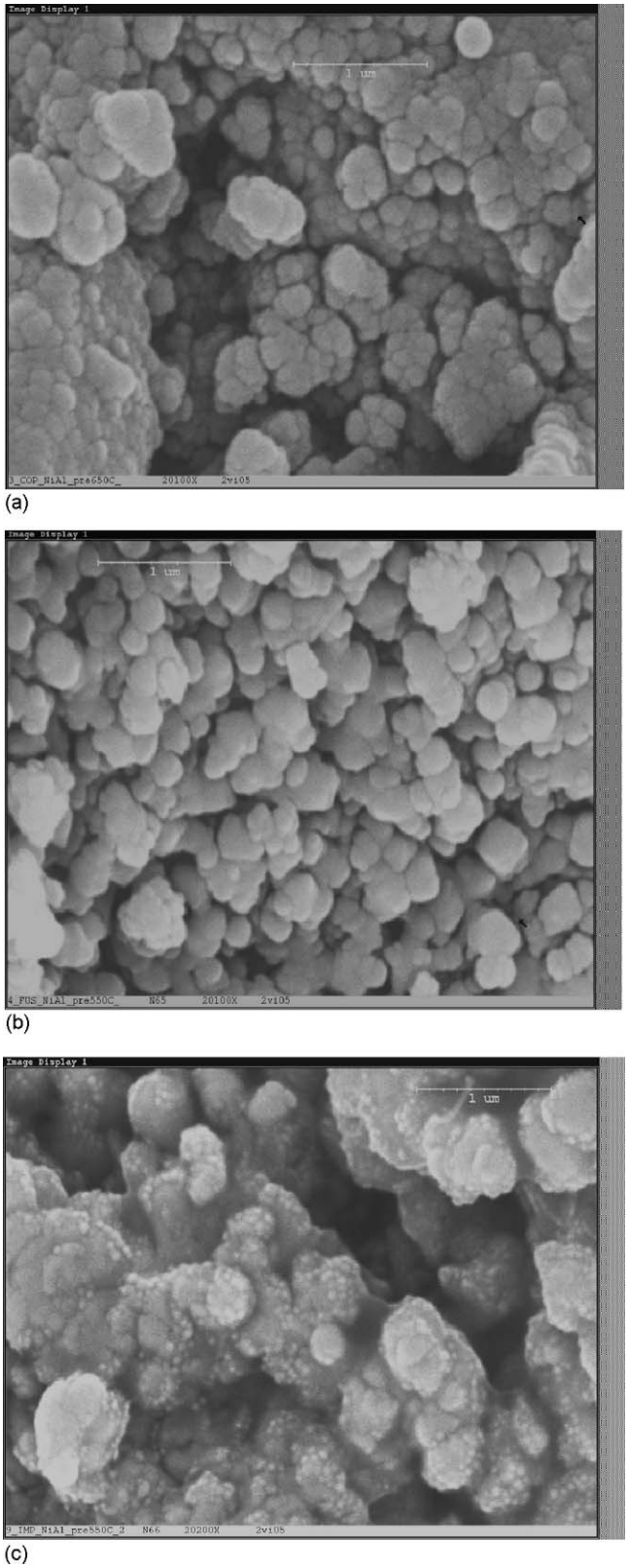

Fig. 2. SEM micrographs of fresh Ni catalysts after reduction pre-treatment prepared by different methods. (a) CopNiAl650. (b) FusNiAl550. (c) ImpNiAl650.

noting that the small domain sizes of NiO achieved in the calcined samples are preserved or even enhanced in Ni after the pre-reducing treatment. The FWHM of the Ni reflections shown in Fig. 1 are highly variable. Co-precipitation NiAl and NiCuAl catalysts show the broadest Ni reflections indicating that their respective Ni domain sizes are small in these samples, in agreement with results obtained in calcined samples shown in Table 1.

The morphological appearance of the fresh catalysts after the pre-reduction treatment is displayed in Fig. 2. All samples appear as large agglomerates of particles with no substantial differences among samples prepared by different methods. The single particles in the agglomerate cannot be resolved and TEM micrographs with higher resolution, shown in Fig. 3(a), reveal that aggregates are rather made of single particles of highly varying size below 50 nm. The largest particles exhibit well-defined polyhedral shapes exposing apparently low-index crystallographic faces. The smallest particles about 1 nm in size, however, show rather rounded shapes, presumably, exposing high-index crystallographic faces. A HREM micrograph of a single particle in Fig. 3(b) shows that it is a single crystal with a lot of planar defects. Consequently, from the TEM study can be deduced that the mean crystal domain size determined by XRD correspond approximately to the single particle shown by TEM.

The degree of Ni dispersion in the fresh catalysts is shown in Fig. 4(a). SEM–EDX line profiles of Ni Kα reveal that the Ni dispersion in the calcined fresh catalysts is highly correlated with the crystal domain sizes determined by XRD. Catalysts prepared by co-precipitation show the highest degree of Ni dispersion while catalysts prepared by impregnation or fusion show the lowest one. The effect of Cu enhancing Ni dispersion is also clearly evidenced through SEM–EDX profiles shown in

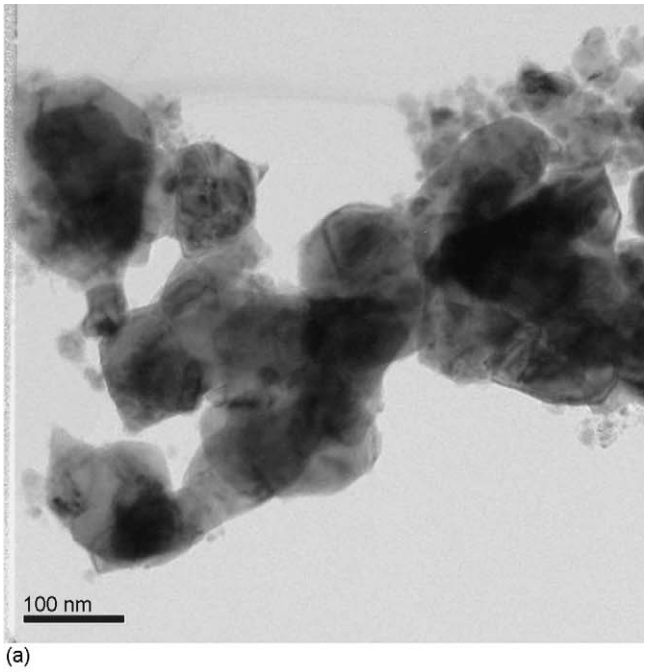

Fig. 3. TEM micrographs of reduced fresh catalyst FusNiAl550. (a) Global appearance at low magnification. (b) HREM micrograph of a single particle.

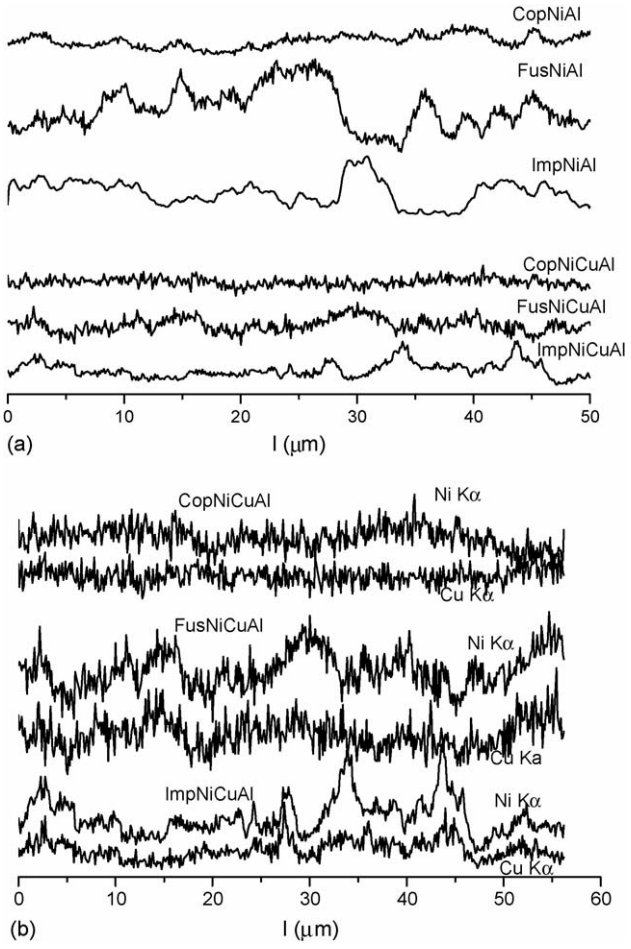

Fig. 4. SEM–EDX line profiles in fresh samples prepared by different methods. (a) Ni Kα line profiles in calcined fresh samples. (b) Ni Kα and Cu Kα in NiCu fresh catalysts after reduction pre-treatment in a hydrogen flow at 550 °C.

Fig. 4(a) by comparing Ni line profiles in NiAl and NiCuAl catalysts. This effect could not be clearly evidenced in the XRD study. Additionally, line profiles of Ni Kα and Cu Kα in NiCuAl in the pre-reduced fresh catalysts (Fig. 4(b)) reveal that Cu is chemically associated to Ni in the reduced fresh catalysts through the formation of an alloy $Ni_{(1-x)}Cu_x$ also not revealed by XRD.

3.2. Hydrogen evolution in tests of catalytic activity

The hydrogen evolution in the outlet gas from the reactor in activity tests at 700 °C is shown in Fig. 5(a and b) for NiAl and NiCuAl catalysts, respectively, prepared by different methods. At start, all catalysts show hydrogen concentrations lower than those expected for thermodynamic equilibrium. The catalytic activity in all cases decreases with time only slightly, in spite of the highly increasing concentration of deposited carbon. It indicates that carbon deposition occurs as long filaments through the proposed mechanisms in which a side of the Ni particle is always exposing active sites available to make the catalytic process go on. From the high differences in Ni domain sizes (Table 1) and degrees of Ni dispersion (Fig. 4), one would expect to observe substantial differences in performance of the fresh catalysts [23]. However, domain size effects on their respective hydrogen evolution were only evidenced for Cu doped catalysts NiCuAl as shown in Fig. 5(b). The presence of Cu increases the catalytic activity as clearly shown by comparing results in Fig. 5(a and b). A recent study of Ni catalysts doped with Cu, Rh, Pd, Ir and Pt showed that only Pd doping increased the Ni activity through an alloying effect [24]. Other studies [15], however, reveal that Cu doping may improve substantially the performance of Ni catalysts although no a plausible explanation of the role of Cu has been given yet. Some studies have shown that Cu is not an active catalyst for the thermal decomposition of methane and even at a high operating temperature of 900 °C no deposited carbon was detected [25]. Consequently, the role of Cu as a dopant is simply to enhance the methane chemisorption on clean Ni surfaces and/or facilitate filament growing through the dilution effect derived from Ni alloying.

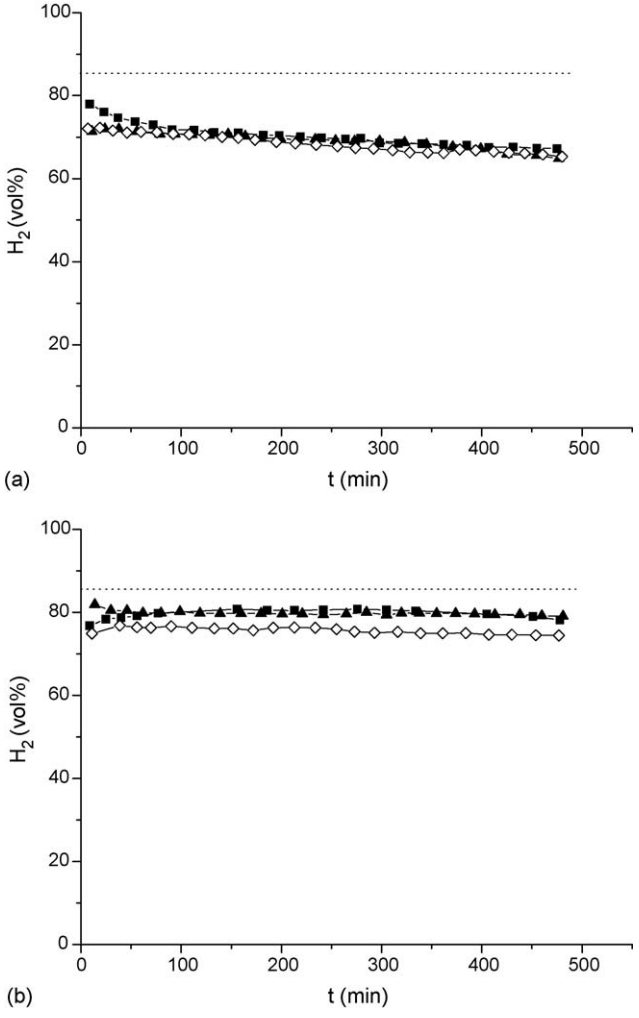

Fig. 5. H_2 evolution in activity tests at 700 °C of catalysts prepared by co-precipitation (▲), fusion (■) and impregnation (◇) activated in H_2 flow at 550 °C. (a) Catalysts NiAl and (b) Catalysts NiCuAl. Equilibrium values shown as dotted lines.

Catalyst deactivation was not reached at the end of the test as shown in Fig. 5. Since among the catalysts tested, substantial differences in the hydrogen evolution were not observed, so great differences in the carbon concentration in used catalysts cannot be expected. The C/Ni weight ratio in used catalysts does not seem to be a useful parameter to measure the catalyst efficiency in this work. Attention in this study, however, has to be drawn to the evolution of structural properties of Ni and that of the deposited carbon in used catalysts.

3.3. Characterization of Ni and deposited carbon in used catalysts after testing

SEM micrographs of used NiCuAl catalysts after activity tests is shown in Fig. 6(a–c). The presence of filamentous carbon a few nanometers in diameter and some micrometers long are clearly evidenced in the three samples. Thicker carbon filaments are apparent in sample CopNiCuAl as compared with those thinner found in samples FusNiCuAl and ImpNiCuAl. The presence of filamentous carbon emerging from Ni particles makes these samples highly inhomogeneous. SEM–EDX line profiles of Ni Kα taken from used catalysts are a visual method to set up clear differences in Ni aggregation, as shown in Fig. 7. Used catalyst CopNiCuAl and, in lower degree, also ImpNiAl are highly inhomogeneous due to the presence of large single particles or agglomerates of Ni. In other used catalysts prepared by fusion, samples FusNiAl and FusNiCuAl, however, the degree of Ni dispersion is comparatively very high. Since the mechanisms proposed in the literature for filament growing suggest that the diameter of carbon fibers must be approximately equal to the Ni particle size, one would expect from data shown in Table 1 obtaining the thinnest carbon fibers in samples prepared by co-precipitation with the smallest particle size, in clear disagreement with experiments. From the SEM–EDX study it must be concluded that Ni undergoes strong particle aggregations during the thermal decomposition of methane at 700 °C. The thickness of the filamentous carbon is not

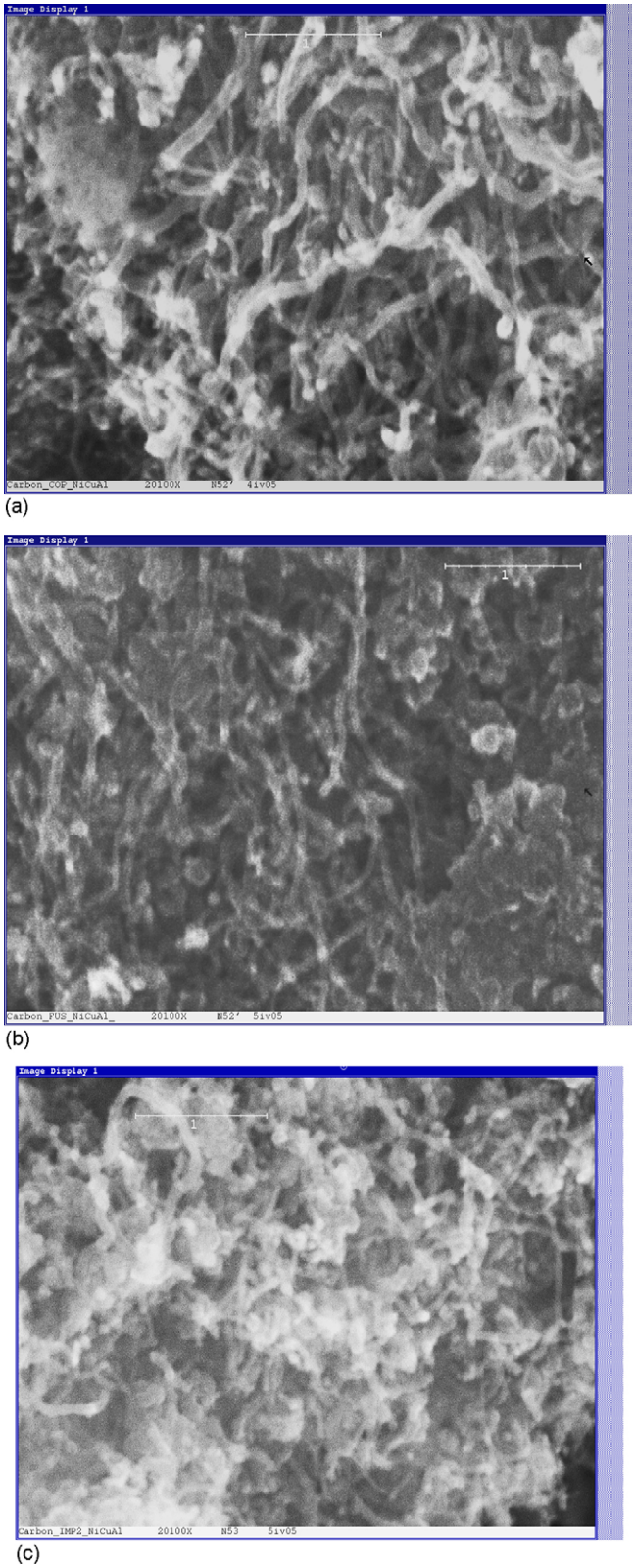

Fig. 6. SEM micrographs of the used NiCu catalysts after activity tests. (a) CopNiCuAl; (b) FusNiCuAl; (c) ImpNiCuAl.

determined by the Ni particle size in the fresh catalyst but in the used catalyst that can be very different.

The involved structural changes of Ni in used catalysts, respect to that found in fresh catalysts, and the structural

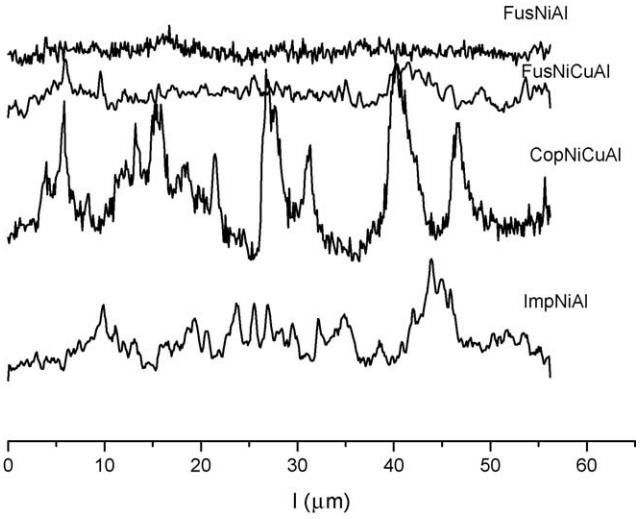

Fig. 7. SEM–EDX line profiles of Ni Kα in used samples.

properties of the deposited carbon have been studied by XRD. Their respective powder XRD patterns shown in Fig. 8 reveal two prominent reflections at 44.34 and 51.75° assigned to metal Ni planes (1 1 1) and (2 0 0), respectively, and a third one at 26.23° assigned to graphite basal planes (0 0 2). The Ni reflections in the patterns of used catalysts are much narrower than those in powder patterns of fresh catalysts (Fig. 1) suggesting that Ni has undergone important changes during the thermal decomposition of methane.

Quantitative data can be obtained from further treatment of the powder XRD patterns by Rietveld methods, as shown in Table 2. By comparing the domain sizes of Ni in used catalysts (Table 2) and those of NiO in the fresh calcined catalysts (Table 1) may be deduced that Ni has undergone substantial thermal sintering during the activity tests. Additionally, the respective reflection C (0 0 2) shows significant shifting towards lower diffraction angles that can be associated to an enlargement of the parameter, *c*, of the hexagonal unit cell of

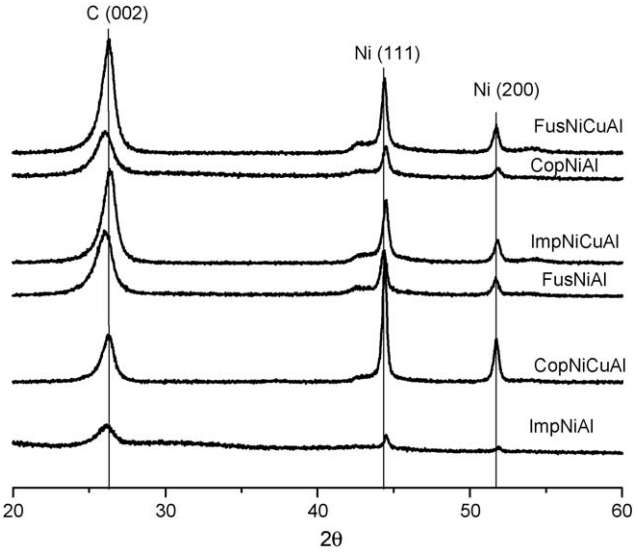

Fig. 8. Powder XRD patterns of used catalysts.

Table 2
Quantitative data from the XRD study of the used catalysts

Samples	C		Ni (domain size (nm))	$(C/Ni)_{wt}$
	$c/2$ (nm)	L_c (nm)		
CopNiAl	0.3420	10.6	–	19.0
FusNiAl	0.3404	12.2	60.0	20.3
ImpNiAl	0.3420	10.6	102.8	13.7
CopNiCuAl	0.3386	16.4	33.8	6.4
FusNiCuAl	0.3393	30.1	61.0	17.9
ImpNiCuAl	0.3391	32.9	39.9	16.9

graphite. The graphene distances, $c/2$, of the deposited carbon in used catalysts go from 0.3386 nm in sample CopNiCuAl to 0.3420 nm in samples ImpNiAl and CopNiAl. For comparison a perfect graphite has interplanar distance of basal planes of 0.3354 nm while interplanar distances of 0.3440 nm have been measured in highly disordered turbostratic carbons, in spite of the apparent inherent inaccuracies introduced in dealing with very small domain sizes [26]. Additionally, the domain size, L_c, of the deposited carbon along the crystallographic direction c varies from 10 to 33 nm. Low values of L_c are highly correlated with high values of the parameter c, as one would expect for a turbostratic carbon. On the other hand, large values of L_c are correlated with small values of the parameter c corresponding to almost perfect graphite. In this sense, it may be concluded that catalysts FusNiCuAl and ImpNiCuAl lead to the formation of a high-order deposited carbon structurally close to a perfect graphite while catalysts prepared by co-precipitation and, especially in the absence of Cu, lead to the formation of a low-ordered deposited carbon. The carbon-to-Ni weight ratio in used catalysts at the end of the test, as a parameter for measuring the catalyst efficiency, is also shown in Table 2. Taking into account the important differences in the Ni domain sizes in the fresh catalysts, one would expect obtaining substantial differences in this parameter among the different catalysts tested. Fixed-time activity tests, however, not showed very high differences in hydrogen evolution and, additionally, all of them remained still active at the end of the test. Consequently, C/Ni weight ratio data for all tested catalysts in Table 2 show no significant differences, except for catalyst CopNiCuAl for which this parameter is very low.

The main conclusions to be derived from the SEM–EDX and powder XRD studies of fresh and used catalysts are that the method of preparation is highly determinant of the size of the Ni particles in the fresh catalysts that, in turn, highly influences the Ni state and the structural properties of the deposited carbon in used catalysts. In particular, the presence of Cu in catalysts FusNiCuAl and FusNiCuAl enhances the formation of thin nanofibers of well-ordered graphitic carbon while CopNiAl and ImpNiAl in the absence of Cu leads to the formation of highly disordered turbostratic carbon.

Raman spectroscopy is a very sensitive technique for carbon characterization to gain information on the structural order along the basal planes in a graphitic carbon. It has been widely used for the characterization of different carbon forms going from highly ordered materials, such us graphite, fullerenes or nanotubes, to highly disordered, such as glassy, black, activated

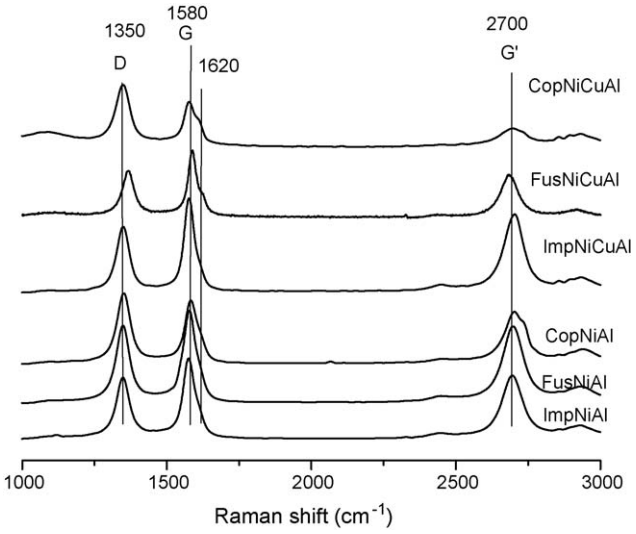

Fig. 9. Raman spectra of Ni and NiCu used catalysts prepared by different methods.

or amorphous carbons [27–29]. In this study, the used catalysts are made of Ni, Cu, Al_2O_3 and deposited carbon, however, none of these compounds except carbon show prominent features in the corresponding Raman spectra. Consequently, the methodology used for characterization of deposited carbon in these used catalysts is similar to that applied in the study of pure carbonaceous materials. Raman spectra of used catalysts, displayed in Fig. 9, show bands G at 1580 cm^{-1}, D at 1350 cm^{-1} and G′ at 2700 cm^{-1} that are very common in defective carbons. Additionally, a shoulder at 1620 cm^{-1} assigned to a maximum in the DOS curve of phonon dispersion also appearing in Raman spectra of defective carbons is also apparent. No other absorption bands are apparent, neither in the range of low frequencies that could be assigned to breathing normal modes in nanotubes, nor others bands located in the intermediate range of frequencies that could be assigned to band splitting in ordered structures with different symmetry than graphite, such as fullerenes or nanotubes. The appearance of the above absorption bands reveals that the deposited carbon from the thermal decomposition of methane is a defective carbon with identical band location in all studied samples. The point defects we are dealing with in Raman spectroscopy are located in the graphene planes (plane a–b) and, consequently, the structural information gained from this technique is complementary of that obtained by XRD. In this last case, most of the structural information gained from the study of carbonaceous materials is in a direction perpendicular to the basal planes (direction c). A measure of defect concentration in the graphemes can be obtained from the intensity ratio of bands D and G as shown in Table 3. The mean crystal domain size along the basal planes of deposited carbon can be determined by applying Tuinstra and Koenig's law:

$$L_a = 4.4\frac{I_D}{I_G}, \quad L_a \text{ in nm}$$

only valid for a laser excitation of 514.5 nm and range of domain size $2.5 < L_a < 300$ nm

Table 3
Raman study of deposited carbon in used catalysts with the intensity ratio of bands D and G and the crystal domain size, L_a, along the basal planes

Samples	I_D/I_G	L_a (nm)
CopNiAl	1.03	4.5
FusNiAl	0.74	3.3
ImpNiAl	0.59	2.6
CopNiCuAl	1.21	5.3
FusNiCuAl	0.63	2.8
ImpNiCuAl	0.66	2.9

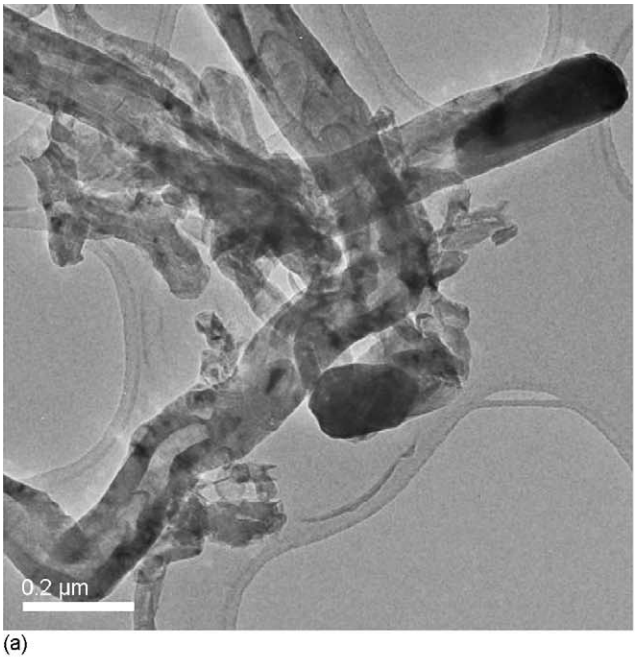

(a)

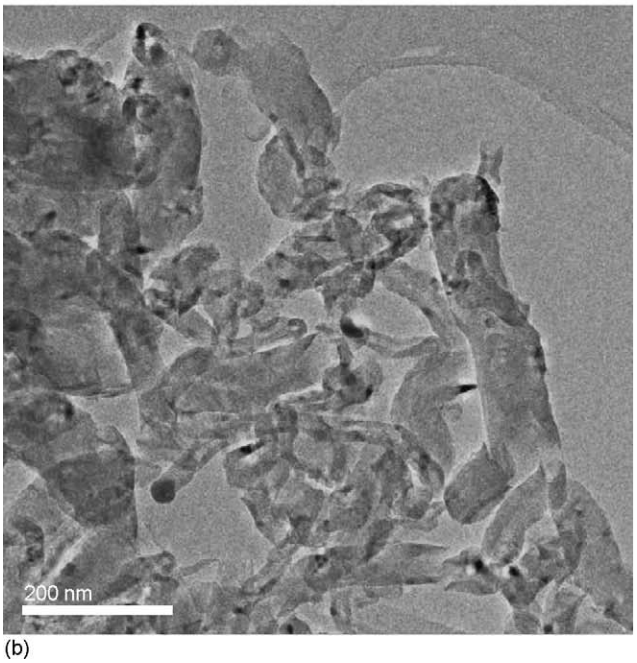

(b)

Fig. 10. TEM micrographs of used catalysts. (a) CopNiCuAl and (b) FusNiCuAl.

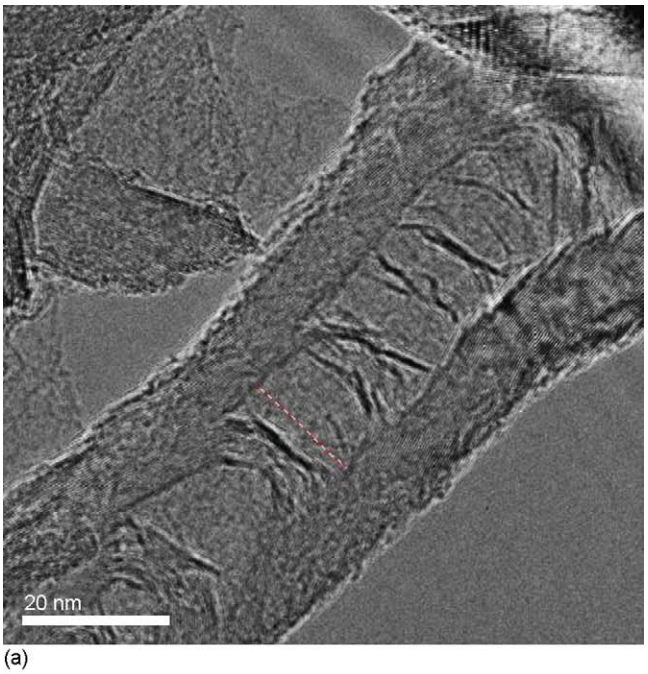

(a)

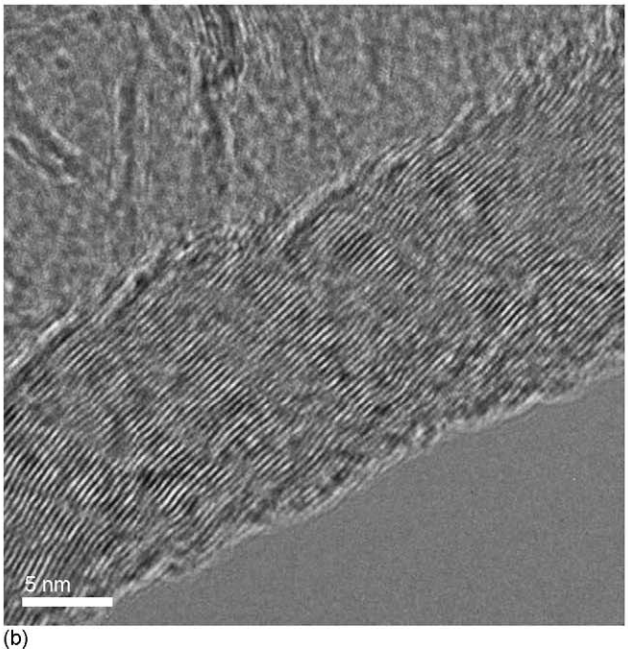

(b)

Fig. 11. HREM of filamentous carbon in used catalyst FusNiCuAl. (a) Detail of two carbon fibers running almost parallel. (b) Detail of a single carbon fiber illustrating the arrangement of the graphenes.

The mean crystal domain sizes along the basal planes L_a in the deposited carbon as determined by Raman spectroscopy (Table 3) is substantially lower than those in a perpendicular direction L_c determined by XRD (Table 2). In this case, L_a seems to be only slightly dependent on the method used for catalyst preparation.

Direct evidence of the involved structural changes in Ni and on the deposited carbon can be gained using TEM with the highest achievable lateral resolution. TEM micrographs of used catalysts CopNiCuAl and FusNiCuAl are shown in Fig. 10(a

and b), respectively. Carbon filaments are made of two thin fibers running almost parallel each other, emerging from a dark Ni particle of about 0.3 μm long (Fig. 10(a)). The Ni particles show a high anisotropy of shape, a rounded appearance at one side and highly enlarged carbon-covered at the other side that is not found in fresh catalysts. Consequently, the presence of these particles exclusively in used catalysts suggest they are formed during the decomposition of methane process through a mechanism including thermal sintering, as evidenced by SEM–EDX and XRD and chemical-induced faceting as deduced from the TEM study. Many smaller Ni particles are also found embedded in long carbon fibers, in which this anisotropy of shape cannot be evidenced. In used catalyst FusNiCuAl (Fig. 10(b)) the dark Ni particles are substantially smaller than in sample CopNiCuAl (Fig. 10(a)) in complete agreement with SEM–EDX results shown in Fig. 7. Additional structural information on the graphene orientation in the deposited carbon can be gained from the HREM micrographs shown in Fig. 11(a and b). Fig. 11(a) is a detailed picture of two nanofibers of deposited carbon around 10 nm in diameter running almost parallel 16 nm apart, that it is the approximate size of the Ni particle giving place to these carbon fiber. The arrangement of graphenes in the right-hand fiber shown in Fig. 11(a) is displayed in Fig. 11(b) at higher magnification forming an angle around 14 with the fiber axis. Within a fiber, the graphemes reach the fiber surface leaving a rough surface. Other graphemes extends up to the other parallel fiber as a bundle of very thin fibers like steps in a staircase. Going along a graphene one finds a lot of structural defects breaking down the graphene periodicity at space intervals (domain size) of around 3–5 nm, in complete agreement with Raman results shown in Table 3.

4. Conclusions

From the study of NiAl and NiCuAl catalysts for the thermal decomposition of methane can be concluded, that the methods of preparation used: Co-precipitation, fusion or impregnation and the presence of Cu in NiCuAl catalysts have a strong influence in the degree of dispersion of Ni and Ni crystal domain sizes in the fresh catalysts. At the operating conditions used, all catalysts show a hydrogen evolution close to that expected from thermodynamics especially NiCuAl catalysts. In spite of the high amount of deposited carbon, at the end of the activity tests (500 min) all catalysts still exhibited almost the same activity than at start. Apparently, they are still far from catalyst deactivation and C/Ni weight ratio is not a sensitive parameter to measure the catalyst efficiency at the end of an activity test. All tested catalysts promote the formation of very long filamentous carbon a few tens of nanometers in diameter some micrometers long but the structural properties of the deposited carbon is especially highly dependent of the presence of Cu as a dopant. NiCuAl catalysts promote the formation of a well-ordered graphitic carbon with relative large crystal domains sizes. NiAl catalysts, however, promote the formation of turbostratic carbon that could be useful as catalyst support or hydrogen storage.

Acknowledgements

This work has been supported with funds provided by the Spanish Ministry of Science and Technology Research Projects PPQ2002-03346 and ENE2005-03801/ALT, and by the Aragon Government through the recognition as a Consolidated Research Group.

References

[1] L.J.M.J. Blomen, M.N. Mugerwa, Fuel Cell Systems, Plenum Press, New York, 1993.
[2] A.J. Appleby, F.R. Foulkes, Fuel Cell Handbook, Krieger Publishing Company, Malabar, FL, 1993.
[3] I. Suelves, M.J. Lázaro, R. Moliner, B.M. Corbella, J.M. Palacios, Hydrogen production by thermo catalytic decomposition of methane on Ni based catalysis: Influence of operation condition on catalyst deactivation and carbon characteristics, J. Hydrogen Energy 30 (2005) 1555–1567.
[4] H.Y. Wang, E. Ruckenstein, Formation of filamentous carbon during methane decomposition over Co-MgO catalysts, Carbon 40 (2002) 1911–1917.
[5] A. Meir, V. Kirilov, G. Kuvshinov, Y. Mogilnykh, A. Steinfeld, A. Weidenkaff, Solar thermal decomposition of hydrocarbons and carbon monoxide for the production of catalytic filamentous carbon, Chem. Eng. Sci. 54 (1999) 3341–3348.
[6] M.A. Ermakova, D.Y. Ermakov, A.L. Chuvilin, G.G. Kuvshinov, Decomposition of methane over iron catalysts at the range of moderate temperatures: The influence of structure of the catalytic systems and the reaction conditions on the yield of carbon and morphology of carbon filaments, J. Catal. 201 (2001) 183–197.
[7] Y. Li, C.L. Chang, Catalytic growth of carbon fibers from methane on a nickel–alumina composite catalyst prepared from a Feitknecht compound precursor, Appl. Catal. A: Gen. 163 (1997) 45–57.
[8] T.V. Choudhary, C. Sivadinarayana, C.C. Chusuei, A. Klinghoffer, D.W. Goodman, Hydrogen production via catalytic decomposition of methane, J. Catal. 199 (2001) 9–18.
[9] P. Wang, E. Tanabe, K. Ito, J. Jia, H. Morioka, T. Shishido, K. Tahekira, Filamentous carbon prepared by catalytic pyrolisis of CH_4 on Ni/SiO_2, Appl. Catal. A: Gen. 231 (2002) 35–44.
[10] M.A. Ermakova, D. Yu, A.L. Ermakov, G.G. Kuvshinov, L.M. Plyasova, New nickel catalysts for the formation of filamentous carbon in the reaction of methane decomposition, J. Catal. 187 (1999) 77–84.
[11] M.A. Ermakova, D.Y. Ermakov, G.G. Kuvshinov, Effective catalysts for direct cracking of methane to produce hydrogen and filamentous carbon. Part I: Nickel catalysts, Appl. Catal. A: Gen. 201 (2000) 61–70.
[12] Y. Li, J. Chen, Y. Quin, L. Chang, Simultaneous production of hydrogen and nanocarbons from decomposition of methane on a nickel-based catalyst, Energy Fuels 14 (2000) 1188–1194.
[13] X. Wang, Y. Jia, Q. Yao, F. Wang, J. Ma, X. Hu, The calculation of the surface energy of high-index surfaces in metals at zero temperature, Surf. Sci. 551 (2004) 179–188.
[14] G.G. Kuvshinov, Y.I. Mogilnykh, D.G. Kuvshinov, Kinetics of carbon formation from CH_4–H_2 mixtures over nickel containing catalyst, Catal. Today 42 (1998) 357–360.
[15] V.B. Fenelonov, A.Y. Derevyankin, L.G. Okkel, L.B. Avdeeva, V.I. Zaikovskii, E.M. Moroz, A.N. Salanov, N.A. Rudina, V.A. Likholobov, S.K. Shaikhutdinov, Structure and texture of filamentous carbons produced by methane decomposition on Ni and Ni-Cu catalysts, Carbon 35 (1997) 1129–1140.
[16] P. Serp, M. Corrias, P. Kalck, Carbon nanotubes and nanofibers in catalysis, Appl. Catal. 253 (2003) 337–358.
[17] W. Arabczyk, W. Konicki, U. Narkiewicz, I. Jasinska, K. Kalucki, Kinetics of the iron carbide formation in the reaction of methane with nanocrystalline iron catalyst, Appl. Catal. A: Gen. 266 (2004) 135–145.
[18] D. Chen, K.O. Christensen, E. Ochoa-Fernández, Z. Yu, B. Totdal, N. Latorre, A. Monzón, A. Holmen, Synthesis of carbon nanofibers: Effects

of Ni crystal size during methane decomposition, J. Catal. 229 (2005) 82–96.
[19] L. Piao, Y. Li, J. Chen, L. Chang, J.Y.S. Lin, Methane decomposition to carbon nanotubes and hydrogen on an alumina supported nickel aeerogel catalyst, Catal. Today 74 (2002) 145–155.
[20] T.V. Reshetenko, L.B. Avdeeva, Z.R. Ismagilov, A.L. Chuvilin, Catalytic filamentous carbon as supports for nickel catalysts, Carbon (2004) 143–148.
[21] G.G. Kuvshinov, Y.I. Mogilnykh, D.G. Kuvshinov, V.I. Zaikovslii, L.B. Avdeeva, Peculiarities of filamentous carbon formation in methane decomposition on Ni-containing catalysts, Carbon 36 (1998) 87–97.
[22] C. Park, M.A. Keane, Catalyst support effects in the growth of structured carbon from the decomposition of ethylene over nickel, J. Catal. 221 (2004) 386–399.
[23] M.L. Toebes, J.H. Bitter, A.J. van Dillen, K.P. de Jong, Impact of the structure and reactivity of nickel particles on the catalytic growth of carbon nanofibers, Catal. Today 76 (2002) 33–42.
[24] S. Takenaka, Y. Shigeta, E. Tanabe, K. Otsuka, Methane decomposition into hydrogen and carbon nanofibers over supported Pd-Ni catalysts, J. Catal. 220 (2003) 468–477.
[25] B.M. Corbella, L. de Diego, F. García, J. Adánez, J.M. Palacios, The performance in a fixed bed reactor of copper-based oxides on titania as oxygen carriers for chemical looping combustion of methane, Energy Fuels 19 (2005) 433–441.
[26] H. Fujimoto, Theoretical X-ray scattering intensity of carbons with turbostratic stacking and AB stacking structures, Carbon 41 (2003) 1585–1592.
[27] W.H. Weber, R. Merlin, Raman Scattering in Materials Science, Springer-Verlag, Heidelberg, Germany, 2000.
[28] M.S. Dresselhaus, G. Dresselhaus, P.C. Eklund, Science of Fullerenes and Carbon Nanotubes, Academic Press Ltd., London, 1995.
[29] R. Saito, G. Dresselhaus, M.S. Dresselhaus, Physical properties of carbon nanotubes, Imperial College Press, London, 2000.